ELSEVIER

Journal of Power Sources 87 (2000) 186–194

JOURNAL OF POWER SOURCES

www.elsevier.com/locate/jpowsour

Characterization of commercial Li-ion batteries using electrochemical–calorimetric measurements

S. Al Hallaj, J. Prakash, J.R. Selman *

Center for Electrochemical Science and Engineering, Department of Chemical and Environmental Engineering, Illinois Institute of Technology, Chicago, IL 60616, USA

Received 18 February 1999; accepted 22 October 1999

Abstract

Commercial Li-ion cells of Type 18650 dimensions and prismatic designs from different manufacturers have been tested to evaluate their performance and to study their thermal behavior using electrochemical–calorimetric methods. All cells tested in this work showed good performance and cyclability under normal operating conditions. The measured heat effect for the cells were exothermic during discharge and partially endothermic during charge. Cell impedance was measured for selected cells and showed some dependence on the state of charge or depth of discharge, with significant increase at the end of discharge due to concentration polarization. The entropy coefficient (dE_{eq}/dT) for the A&T (18650) and Panasonic (CGR 18650) cells were measured using potentiometric methods at different depths of discharge (DOD). The measured values for both cells showed some dependence on the DOD with some perturbation near 4.0 V, where the measured dE_{eq}/dT for Panasonic cell had an unexpected positive value. This was found to be consistent with the measured endothermic heat effect during discharge for the Panasonic cell near $E_{eq} = 4.0$ V. This may be related to a phase change in the $LiCoO_2$ cathode material, as reported in the literature, and to structural transformation in the graphite used as anode material, in the Panasonic cell.

Keywords: Li-ion batteries; Electrochemical measurements; Accelerated rate calorimeter

1. Introduction

Lithium-ion batteries possess high energy density compared to other secondary batteries. Small Li-ion batteries with a capacity of 1300 to 1900 mA h are currently commercially available to power portable electronic devices such as camcorders, computers, cameras, etc. In addition, Li-ion batteries as power sources for electric vehicles (EV) are being developed to provide longer driving range, higher acceleration, and long lifetime. However, safety concerns of the Li-ion batteries have limited their full utilization in EV applications. The primary challenge in designing an EV lithium-ion battery is its safety under abusive as well as normal operating conditions. The normal operating conditions involve over-discharge, resistive and/or forced over-discharge. Abuse conditions involve shorting, crushing, or excessive overcharging.

Yoda and Ishihara (1997) described a significant role for Li-ion batteries in a battery-based society in the next century. Commercial Li-ion batteries from several manufacturers such as Sony, A&T Battery, and Panasonic are available in the market. However, further development and cost reduction are required to design larger sizes of these batteries suitable for EV and energy storage (load conditioner) applications.

Several researchers [3–6] have evaluated the effect of different designs and materials used in cells on the performance of commercial Li-ion cells. However, most of the work reported in the literature is limited to cylindrical cells and little research has been focused on the thermal behavior and its effect on the performance of these cells.

In this work we present electrochemical–calorimetric measurements using a number of commercial Li-ion cells with different chemistries and designs, for different cycling rates at 35°C operating temperature. Cells were taken from camcorder or cellular phone packs available in the market. The ARC–Arbin experimental set-up is used to measure the temperature, voltage and current of the cells at differ-

* Corresponding author. Tel.: +1-312-567-3970; fax: +1-312-567-6914; e-mail: selman@charlie.cns.iit.edu

0378-7753/00/$ - see front matter
PII: S0378-7753(99)00472-3

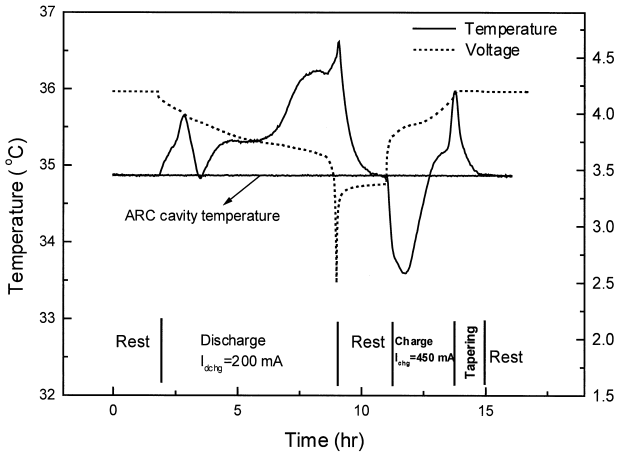

Fig. 1. Schematic of an ARC–Arbin experiment during a charge/discharge cycle.

ent charge/discharge rates. Measurements are taken during cycling over a range of operating parameters within the limits recommended by the manufacturer [2]. The instantaneous heat generation rate, its correlation with the cell impedance, and its dependence on the discharge rate are of special interest. In previous work [1], it was found that in the temperature range 35–55°C used in these measurements, the operating temperature has relatively little effect on the heat generation rate. Therefore, in this work, the operating temperature is limited to 35°C only.

2. Experimental set-up and procedure

The heat effect of a commercial Li-ion cell (Sony US18650) was measured using an Accelerating Rate Calorimeter (ARC 2000, Columbia Scientific Industries, Austin, TX) in combination with a battery cycler (Model BT 2042, Arbin Instruments, College Station, TX), details for the ARC–Arbin experimental set-up are described elsewhere [1]. The ARC–Arbin set-up was slightly modified for this work by using the ARC–bomb thermocouple for cell temperature measurements instead of the Keithley 2000, and not using insulation around the cell. The simplified ARC–Arbin set-up was used in this work to test a number of commercially available Li-ion cells from different manufacturers. Schematics of an ARC–Arbin experiment are shown in Fig. 1. 18650 cells from three different manufacturers (Sony, Panasonic and A&T) and two prismatic A&T cells (600 and 1600 mA h) were tested to study the effect of capacity and geometry on the thermal behavior. Chemistries and specifications of the cells are listed in Tables 1 and 2, respectively.

The cells were cycled galvanostatically in the anodic (4.2 V) and cathodic (2.5 V) directions during charge and discharge, respectively. The charge/discharge capacities of all cells were measured at different charge/discharge rates (C-rates). All cell were cycled 10 and 5 consecutive times at C/3 and C/6 charge/discharge rates, respectively, in order to measure their capacities and evaluate their performance (Table 3).

Measurements presented here were taken for selected cells of each type. Occasional tests of other cells of the same type did not show any significant deviation so the cell chemistry and design were considered similar for all cells of the selected cell type. However, it was noted that cell manufacturers keep changing their cell chemistries even for the same cell design and application. For example, Li-ion cells used in the Sony camcorder batteries have been changed three times over the past two years. Initially, Sony used their own (Type US 18650) Li-ion cells of 1.35 A h capacity in the Sony NP-510 camcorder battery pack [1]. Recently, Sony used Panasonic (Type CGR 18650) cells of 1.4 A h capacity in the NP-520 battery pack [13], while cells tested in this work which were taken from a Sony NP-F550 battery pack were actually Panasonic cells (Type CGR 18650H) of 1.5 A h capacity. All Panasonic and Sony cells have $LiCoO_2$ as cathode electrodes. Sony cells have coke as anode material while Panasonic cells have graphite [4]. In this work, to assure that cells of the same type have the same chemistry, we chose cells with the same production batch number or from the same battery pack.

2.1. Impedance measurements

Current interruption (DC-impedance technique) was used to measure the cell overvoltage at different depths of discharge (DOD). The discharge current was $I = 10$ mA (C/60 rate) for the A&T (600 mA h) cell, and $I = 50$ mA (C/28 rate) for the Panasonic (CGR 18650) and the A&T (18650) cells. After each current interruption, the cell was left to relax for 3 h at open circuit. The instantaneous voltage drop (ΔV_i) was measured after 0.1 s of current

Table 1
Chemistries and applications of Li-ion test cells

Manufacturer	PE material	NE material	Separator	Electrolyte	Application
Sony	$LiCoO_2$	coke	polypropylene /polyethylene	$LiPF_6$/PC +DEC	commercial (camcorders)
Panasonic (Matsushita)	$LiCoO_2$	graphite	polyethylene	N/A	commercial (camcorders)
A&T	$LiCoO_2$	graphitized carbon fiber	polyethylene	N/A	commercial (cell phones)

Table 2
Specifications of Li-ion test cells

Manufacturer	Cell type (size)	Nominal capacity (mA h)	Energy density (A h/l)	Dimensions (mm)
Sony	US18650	1350	81.6	cylindrical 18×65 ($D \times L$)
Panasonic (Matsushita)	CGR 18650H	1500	84.6	cylindrical 18×65 ($D \times L$)
A&T	18650	1350	84.6	cylindrical 18×65 ($D \times L$)
A&T	462905	600	90.0	rectangular $46 \times 29 \times 5$ ($H \times W \times D$)
A&T	463312	1600	87.8	rectangular $46 \times 33 \times 12$ ($H \times W \times D$)

interruption, while the cell voltage drop during relaxation (ΔV_{rel}) was measured every minute. A schematic of the current interruption experiment is shown in Fig. 2. It was not possible to take measurements at higher sampling rate (< 0.1 s) because of instrument limitations of the Arbin cycler. The instantaneous voltage drop (ΔV_i) is mainly due to the ohmic resistance of the cell and partially due to the concentration polarization. The voltage drop due to ohmic resistance is a very fast process, characteristic of electron flows that take place in picoseconds. A high-frequency data acquisition system (MHz) or an oscilloscope is required to capture the actual ohmic voltage drop in this step. The relaxation voltage drop (ΔV_{rel}) corresponds mainly to concentration polarization in the liquid electrolyte and in the solid electrode materials. Especially the latter is a very slow process, characteristic of solid state ionic diffusion. The instantaneous impedance (R_i) and the relaxation impedance (R_{rel}) were estimated using Eqs. (1) and (2), respectively.

$$R_i = \frac{\Delta V_i}{I} \quad (1)$$

$$R_{rel} = \frac{\Delta V_{rel}}{I}. \quad (2)$$

2.2. ARC-method of calibration

At first [1], and in order to estimate the heat dissipation rate from the Sony cell to the calorimeter cavity, we determined the calorimeter constant ($\kappa = 3.84 \pm 0.01 \times 10^{-2}$ W K^{-1}). The ARC constant (κ), is the product of the effective heat transfer coefficient times the surface area of the cell (hA). The value reported above is unique for the Sony cell experiments but has different values for different cell designs and dimensions. In this part of the work, to avoid repetitive ARC constant measurements for each type of cell, we measured the effective heat transfer coefficient (h) directly; using transient temperature measurements for a test cell blank located inside the ARC cavity. An aluminum cylinder with the same dimensions as the Sony (Type US18650) cell was used as a test-cell in these measurements. The ARC temperature was increased at each step, while recording the temperature of the test-cell during that period. The governing equation for this process is given in Eq. (3). It is the energy balance for a lumped heat transfer system (uniform-temperature body) under natural convective heating or cooling conditions, valid for a Biot number less than 0.1 ($Bi < 0.1$).

$$mC_p \frac{dT}{dt} = hA(T - T_a). \quad (3)$$

With initial condition:

$$T = T_a \quad \text{at } t = 0. \quad (4)$$

Here, m is the mass of the cell (kg), C_p the heat capacity (J kg^{-1} K^{-1}), T the cell temperature (K), T_a the ambient temperature (K), t time (s), h the effective heat transfer coefficient (W m^{-2} K^{-1}), and A the cell surface area (m^2).

The solution for Eqs. (3) and (4) is:

$$\ln(\theta) = st. \quad (6)$$

Here:

$$\theta = (T - T_a) \quad (7)$$

$$s = \frac{hA}{MC_p}. \quad (8)$$

The temperature measurements of the aluminum test-cell were plotted against time as shown in Fig. 3. The surface area, heat capacity, and weight of the Al test-cell are 3.674×10^{-3} m^2, 900 J kg^{-1} K^{-1}, and 47.3 g, respectively. The slope (s) of the $\ln(\theta)$ vs. time plot, at each heating step, was estimated using linear regression. An

Table 3
Cell capacity, capacity fading and tapering effect at C/3 and C/6 cycling rates

Manufacturer (cell type)	Measured capacity[a] (mA h) charge/discharge rate	
	C/3	C/6
Sony (US18650)	1201.5	1282.5
Panasonic (CGR 18650H)	1564.5 ± 1	1550.7 ± 3
A&T (18650)	1395.4 ± 2	$1398.6 + 1.1$
A&T 462905	533.2 ± 3.2	542.7 ± 1.7
A&T 463312	1501.1 ± 5	$1493.8 + 4.3$

[a]Average values estimated from the first 10 cycles at C/3 discharge rate followed by 5 cycles at C/6 discharge rate.

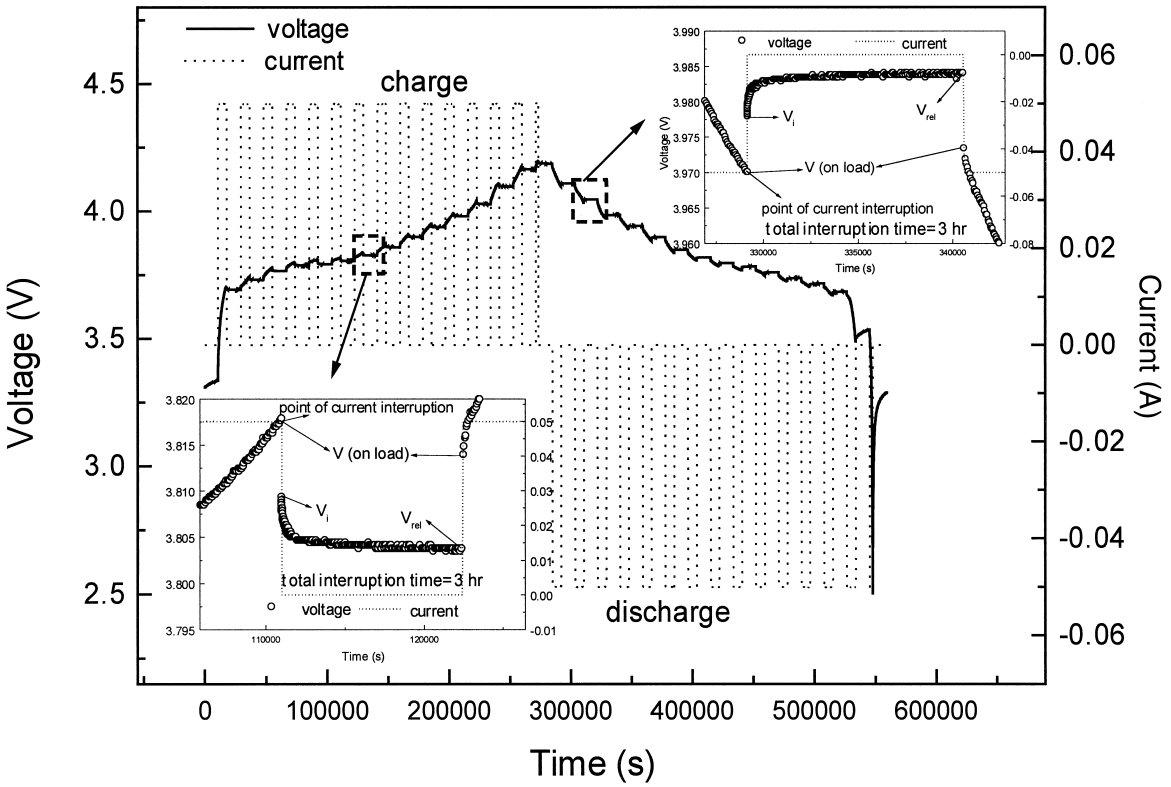

Fig. 2. Schematic of the DC-impedance (current interruption) technique.

average h value of 6.4 ± 0.1 (W m^{-2} K^{-1}) was found for three heating steps measurements, results are shown in Fig. 4. The ARC constant (α_{ARC}) for the Sony cell calculated from this average h value is $2.35 \pm 0.03 \times 10^{-2}$ W K^{-1}, values of the ARC constants (α_{ARC}) for all cells in this part of the work are listed in Table 4. The difference between this estimated value for α_{ARC} and the κ value ($3.84 \pm 0.01 \times 10^{-2}$ W K^{-1}) determined in the earlier Sony cell experiments [1], arises because in the earlier experiments the cell was placed inside a closely fitted cylindrical sheath of Styrofoam in the center of the calorimeter cavity. This insured that the heat generated by the cell was dissipated by conduction only through the insulation material. In this work, the cell was *not* insulated and the heat generated inside the cell is convected to the surrounding air inside the ARC cavity. The cell top and bottom were insulated using thick layers of Teflon on both planar surfaces, which limits the heat dissipation via these surfaces so only the curved side surface is involved.

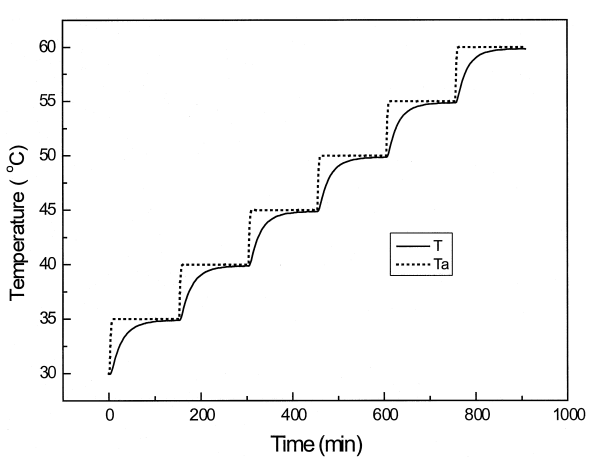

Fig. 3. Schematic of ARC calibration experiment with the Al test cell.

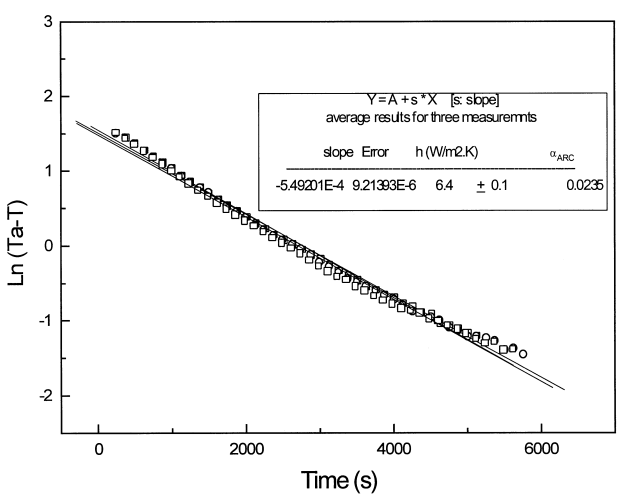

Fig. 4. Linear regression results to estimate the effective heat transfer coefficient inside the ARC.

Table 4
Estimated ARC constants (α_{ARC}) for all cells

Cell	Panasonic CGR 1865H	A&T 18650	A&T 0.6 A h	A&T 1.6 A h
A (m^2)	3.674×10^{-3}	3.674×10^{-3}	3.128×10^{-3}	4.140×10^{-3}
α_{ARC} (W K^{-1})	2.352×10^{-2}	2.352×10^{-2}	2.002×10^{-2}	2.650×10^{-2}

2.3. Calorimetric measurements

The ARC–Arbin set-up was used to measure the temperature rise and heat dissipation rate during charge/discharge. In each experiment, the cell was placed inside the ARC cavity using a specially designed cell holder. The cell was connected to the Arbin cycler using extension wires connected to the cell negative and positive poles at one end and to an Arbin channel cable at the other. Unlike the case in the Sony cell measurements, the ARC cavity temperature was kept at 35°C during all the experiments described in this part of work. The ARC–bomb thermocouple was attached to the cell surface to measure its temperature change during cycling at different charge/discharge rates. Eq. (5) was used to estimate the instantaneous heat dissipation rate (q_d):

$$q_d = \alpha_{ARC} \Delta T \quad (5)$$

Here, α_{ARC} (W K^{-1}) is the ARC constant for each cell, and ΔT (K) is the instantaneous temperature difference between the cell surface and the ARC cavity.

The same experimental set-up was also used to measure the entropy coefficient (dE_{eq}/dT) at different depths of discharge (DOD) for selected cells. The entropy coefficient (dE_{eq}/dT) of the Panasonic (CGR 18650H) and the A&T (18650) cells were determined by measuring the equilibrium potential (E_{eq}) as a function of temperature. The cell temperature was increased stepwise and, at each step, kept constant for 6 h while measuring the cell voltage during that period, as shown in Fig. 5 for the Panasonic cell.

When the cell was fully charged or discharged, we were not able to obtain reliable measurements by increasing the temperature step-wise as explained earlier. Therefore, we used ramp temperature increase (0.2°C/min) combined with instantaneous equilibrium potential measurements. The E_{eq} measurements obtained here were plotted against time and the corresponding (dE_{eq}/dT) values were obtained by dividing the slope of E_{eq} vs. time (minute) by the temperature ramp rate. It is worth mentioning that the entropy coefficient experiments presented in this work took about 6 weeks for each cell.

To assess the reproducibility of the calorimetric measurements, experiments were repeated twice in all cases and the results for both measurements were within the range of experimental error.

3. Results and discussion

3.1. Evaluation of the cells performance

Fig. 6 shows a typical voltage profile against the utilized capacity for the Sony, Panasonic and A&T 18650 cells at C/6 discharge rates. A voltage plateau was noted for the Panasonic and A&T cells during most of the discharge period, while the Sony cell showed a steep voltage slope. This may due to the different types of anode material used in those cells, where Sony has coke, while Panasonic and A&T have graphite and graphitized carbon fibers, respectively. Panasonic had the highest utilized capacity followed by A&T, while the Sony cell had the lowest. The cell voltage at low DOD for the Sony cell was

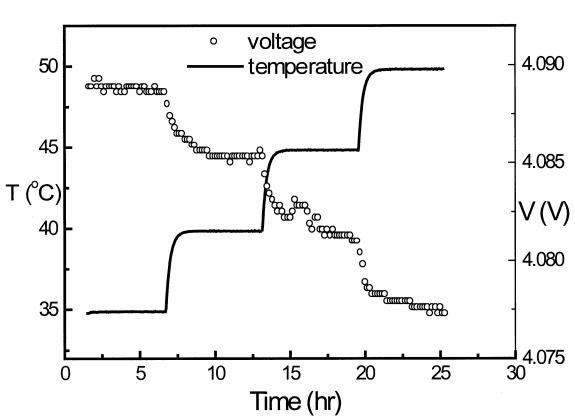

Fig. 5. Schematic of temperature and voltage measurements for the entropy coefficient experiment.

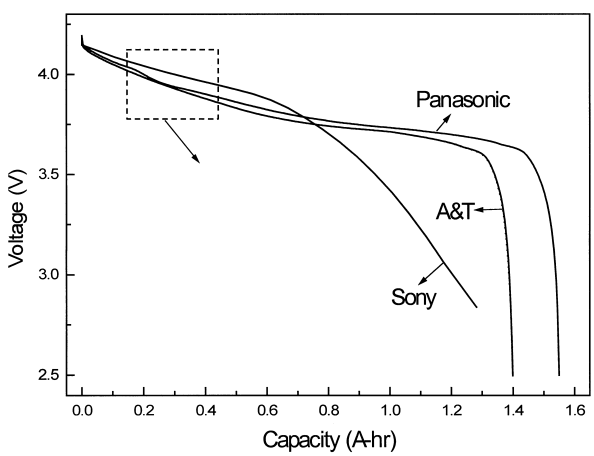

Fig. 6. Voltage profiles for all three 18650 cells during discharge at C/6 rate.

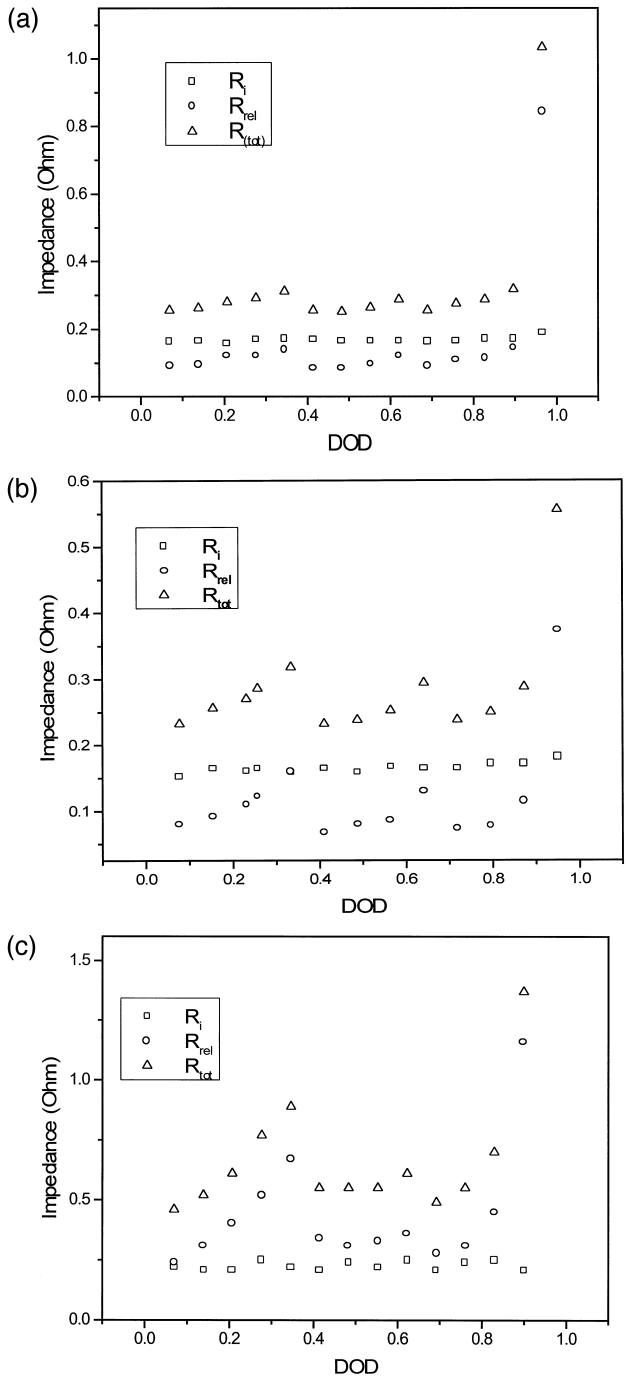

Fig. 7. (a) Impedance measurements for Panasonic (CGR 18650) cell during discharge at $I = 50$ mA. (b) Impedance measurements for A&T (18650) cell during discharge at $I = 50$ mA. (c) Impedance measurements for A&T (600 mA h) cell during discharge at $I = 10$ mA.

significantly higher than that for both Panasonic and A&T cells, then dropped significantly towards the end of discharge. A voltage ripple was observed for the Panasonic cell only between 0.10 and 0.25 A h capacities. This may be due to structural or phase changes in the anode or the cathode materials, respectively. The utilized capacity for the Panasonic and A&T cells was not noticeably changed after the fifth and the ninth cycles, respectively. However, the measured capacity for the Panasonic cell after 50 cycles dropped to near 1.375 A h.

In this work, an additional charging step at constant voltage (tapering) was used after the constant current charging step. During this tapering charge step, the cell voltage was kept constant at 4.2 V until the current dropped below 25 mA. Following charging at C/3 rate, this yielded an additional 11.0% and 19.4% of capacity for the Panasonic (CGR 18650H) and the A&T (600 mA h) cell, respectively. At C/6 cycling rate, the capacity additions due to tapering were 4.8% and 7% for the same cells, respectively.

3.2. Impedance measurements

The impedance measurements for the Panasonic (CGR 18650H), A&T (18650), and A&T (600 mA h) cells are shown in Fig. 7a to c, respectively. The instantaneous impedance was almost the same for each cell at the same depth of discharge or state of charge, during both charge and discharge, for all three cells. However, a significant increase in the relaxation impedance was noted at the end of discharge for all cells. This appears to be due to a build-up of concentration polarization, which usually increases significantly with depth of discharge [8–12]. A slight increase followed by a sudden decrease in the instantaneous (ohmic) impedance was noticed for the Panasonic and A&T cells, at DOD 0.3–0.4 and cell voltage 3.9–4.1 V. This may be due to a phase change in the positive electrode material ($LiCoO_2$) or to structural transformation in the negative electrode (graphite), as will be discussed in more detail elsewhere [13].

During galvanostatic (constant current) charge or discharge, the measured cell voltage is higher than the open circuit potential during charge, and lower than the open circuit potential during discharge. The difference, termed

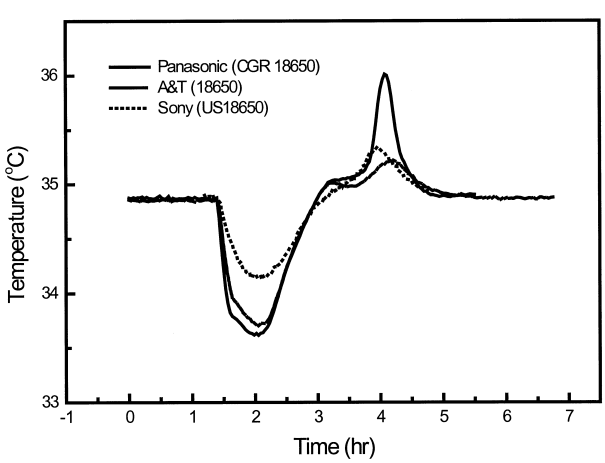

Fig. 8. Temperature profile for different commercial cells of 18650 type during charge at C/3 rate.

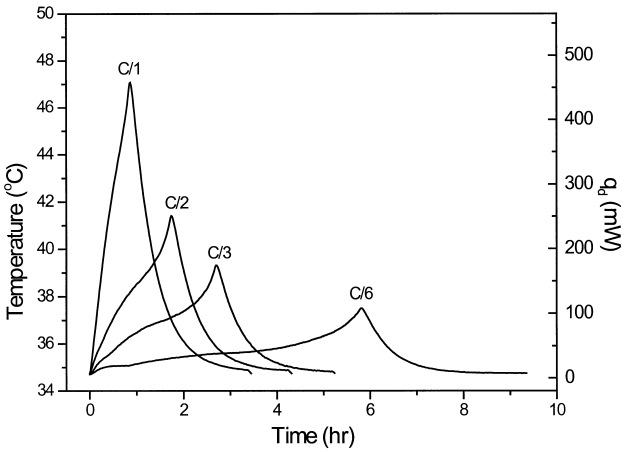

Fig. 9. Temperature and heat dissipation rate for Sony (Type US18650) cell at different *discharge* rates.

overvoltage, results from ohmic resistance, polarization, and other irreversibilities. Consequently, the cell does not reach the fully charged or discharged state when the charge, respectively, discharge cutoff voltage is reached. The cell is not perfectly cyclable and its theoretical capacity (according to Faraday's law) is not fully utilized.

3.3. Heat dissipation rates and temperature measurements

Fig. 8 shows the temperature profile for all 18650 cells during charge at $C/3$ rate followed by charge at constant 4.2 V potential. A strong cooling effect during charge was noted at small state-of-charge, followed by a weak exothermic effect at the end of charge. This is due to the endothermic effect of the deintercalation of Li ions from the positive electrode (Li_xCoO_2) accompanied by intercalation in the negative electrode (carbon or graphite). Measurements of the Sony cell, reported earlier [1], showed that the entropic heat effect is significant, being highly exothermic during discharge and endothermic during charge. These measurements also showed that the entropy

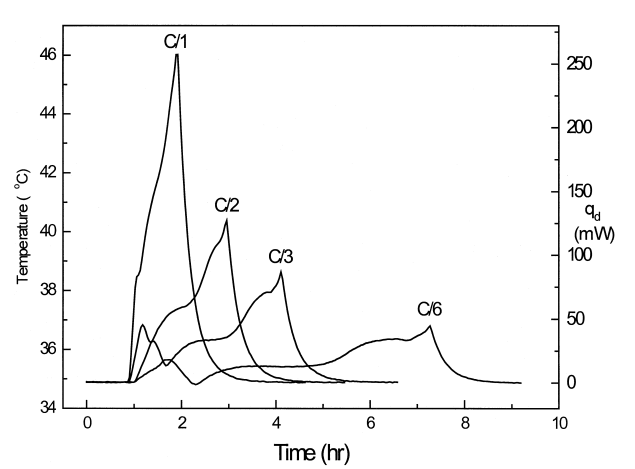

Fig. 10. Temperature and heat dissipation rate for Panasonic (CGR 18650H) cell at different *discharge* rates.

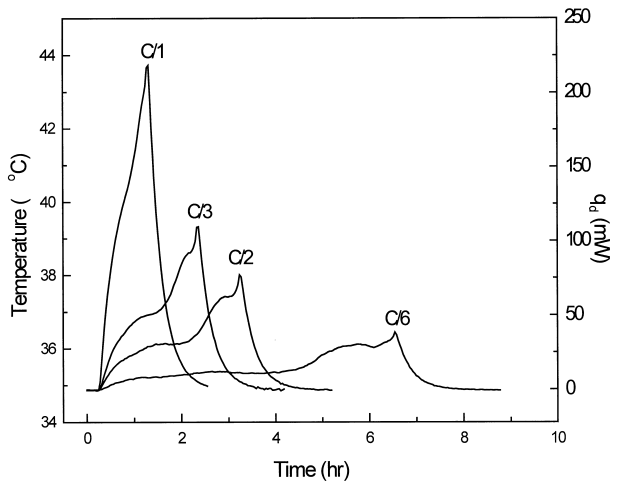

Fig. 11. Temperature rise and heat dissipation rate for A&T (18650) cell at different *discharge* rates.

coefficient (dE_{eq}/dT) was significantly higher at low SOC (high DOD). As a result, the endothermic effect due to entropy of reaction is more dominant at the beginning of charge, while at the end of charge ohmic and polarization impedance increase significantly, and surpass the entropy effect, hence, a net exothermic effect is observed.

Fig. 9 shows the temperature rise and heat dissipation rates for the Sony (Type US18650) cell during discharge at different rates. The instantaneous heat generation rates and the temperature rise were found to be strongly dependent on the rate of discharge. This is consistent with the significant increase in area-specific-impedance (ASI) at the end of discharge, as reported earlier [1]. Fig. 10 shows similar measurements for the Panasonic cell. A significant endothermic effect is noticeable at small DOD for all discharge rates. This may be due to phase transition in the cathode or structural transformation in the graphite anode material, as discussed in more detail elsewhere [13]. Fig. 11 shows the temperature rise and heat dissipation rate for

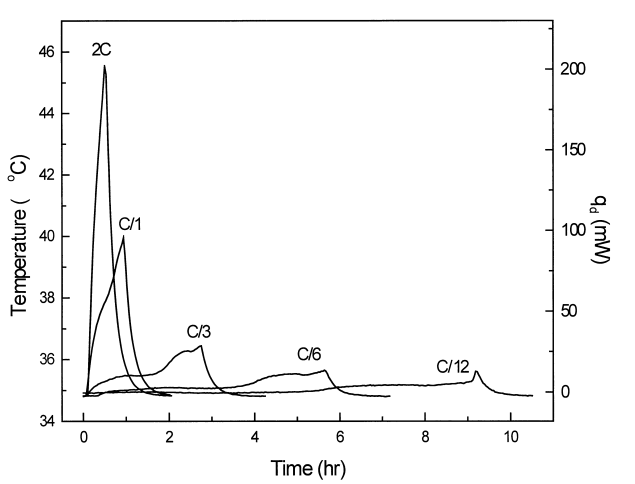

Fig. 12. Temperature rise and heat dissipation rate for A&T (600 mA h) cell at different *discharge* rates.

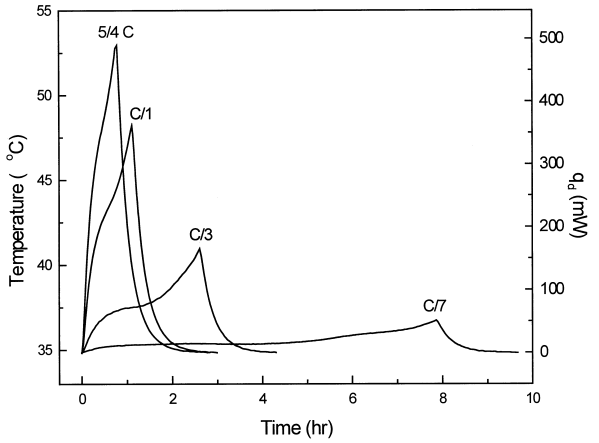

Fig. 13. Temperature rise and heat dissipation rate for A&T (1600 mA h) cell at different *discharge* rates.

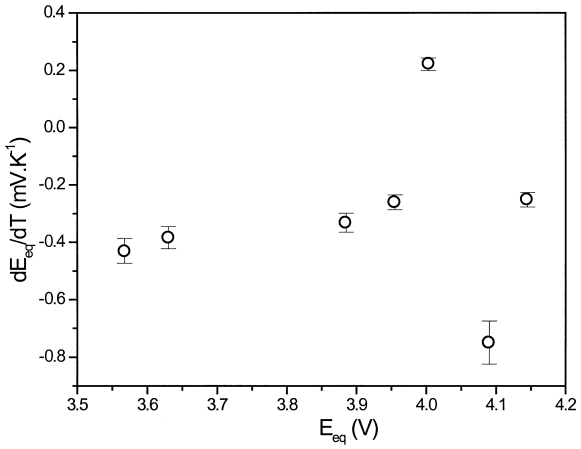

Fig. 15. Entropy coefficients (dE_{eq}/dT) vs. E_{eq} for Panasonic (CGR 18650H) cell.

the A&T (18650) cell during discharge. Similar results are shown in Figs. 12 and 13 for the (600 mA h) and (1600 mA h) A&T cells, respectively. A strong effect of the discharge rate on the temperature rise and heat dissipation rate was noticed for the Panasonic cell and all A&T cells. A sharp temperature increase at the end of discharge, noted for all cells, is due to the sharp increase of cell impedance at the end of discharge.

3.4. dE_{eq}/dT coefficient

From the E_{eq} vs. temperature plots, as shown in Fig. 3, dE_{eq}/dT values were determined, as shown in Fig. 14. Figs. 15 and 16 show the dE_{eq}/dT values determined at different DOD for the Panasonic (CGR 18650H) and the A&T (18650) cells, respectively. Results for the Panasonic cell showed that the entropy coefficient changes sign *from negative to positive* very near $E_{eq} = 4.0$ V. At $E_{eq} = 4.003$ V, $dE_{eq}/dT = +2.73 \pm .25 \times 10^{-4}$ V/K, while dE_{eq}/dT was negative for all other E_{eq}. This may be due to a phase change in the cathode and to a structural change in the anode material. Results for the A&T cell showed that the entropy coefficient is negative at all DOD. For both cells, the entropy coefficient showed some dependence on the depth of discharge. This may be due to changes in the cell chemistry at different DOD. The negative dE_{eq}/dT values indicate that the entropic heat effect is exothermic during discharge, and endothermic during charge, for all charge and discharge rates.

Earlier [1], values of -0.429 and -0.753 mV K^{-1} were reported for the Sony (Type US18650) cell at $E_{eq} = 4.044$ and 3.227 V, respectively. Chen and Evans [6] reported $dE_{eq}/dT = -0.414$ mV K^{-1}, averaged over a range of SOC, and based on data for the Sony cell reported by Saito et al. [5]. Kanari et al. [7] reported detailed measurements for the Sony (Type US18650) cell at different DOD. Their results showed negative dE_{eq}/dT values for all DOD, and a strong dependence on the state of charge. For example, dE_{eq}/dT varied from -0.24 to -0.63 mV K^{-1} over the range of 0–1.0 DOD.

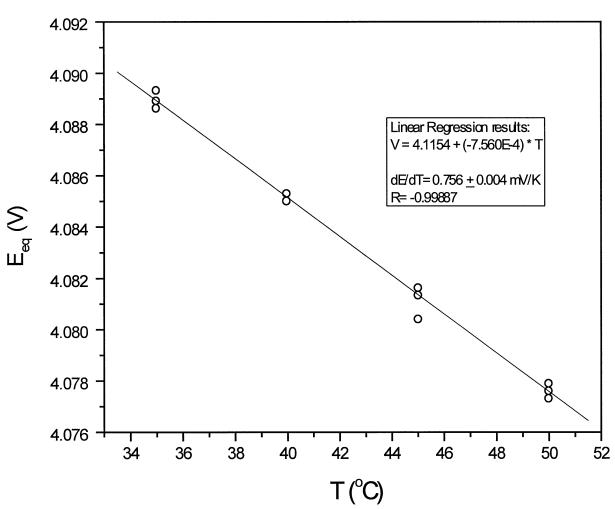

Fig. 14. Linear regression results for E_{eq} vs. temperature for entropy measurements for Panasonic (CGR 18650H) cell at OCV = 4.09 V.

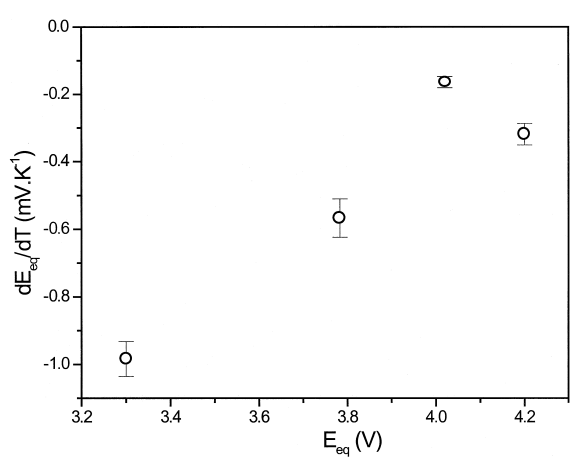

Fig. 16. Entropy coefficients (dE_{eq}/dT) vs. E_{eq} for A&T (18650) cell.

4. Conclusions

Different commercial Li-ion cells were cycled up to 40 times in some cases to evaluate their performance and measure their capacity, impedance, entropy coefficients, and heat dissipation rates at different charge/discharge rates. The Sony, Panasonic and A&T cells have demonstrated good cyclability and have a long lifetime. The heat dissipation rate for all cells showed a strong dependence on the rate of discharge and increased significantly toward the end of discharge, due to the increase of polarization at the end of discharge. Heat effects for all cells were exothermic during discharge but had an appreciable endothermic effect during charge. This is due to the entropic heat effect, (endothermic during charge and exothermic during charge), which is large relative to the irreversible heat effect under typical load conditions (less than C/3 rate).

A significant temperature drop at 0.23 DOD was noted for the Panasonic (CGR 18650H) cell during discharge at different discharge rates. This was inferred to be due to phase change in the cathode material, or structural transformation in the graphite anode material.

References

[1] J.S. Hong, H. Maleki, S. Al Hallaj, L. Redey, J.R. Selman, J. Electrochem. Soc. 145 (1998) 1489–1501.
[2] Sony Type (US18650) Lithium-Ion Battery Manual, Sony, 1993.
[3] P. Arora, R.E. White, M. Doyle, J. Electrochem. Soc. 145 (1998) 3647–3667.
[4] B.A. Johnson, R.E. White, J. Power Sources 70 (1998) 48–54.
[5] Y. Saito, K. Kanari, K. Kanari, 8th International Meeting of Lithium Batteries, Nagoya, Japan, I-C-15, 1996.
[6] Y. Chen, J.W. Evans, J. Electrochem. Soc. 143 (1996) 2708–2712.
[7] K. Kanari, K. Takano, Y. Saito, Bull. Electrochem. Lab. 60 (1996) 65–75.
[8] K. Kanari, K. Takano, Y. Saito, T. Masuda, Proceedings of International Workshop on Advanced Batteries (Lithium Batteries), AIST, MITI, Osaka, Japan, February 1995.
[9] R. Fong, U. von Sacken, J.R. Dahn, J. Electrochem. Soc. 137 (1990) 3647–3667.
[10] Z.X. Shu, R.S. McMillan, J.J. Murray, J. Electrochem. Soc. 145 (1998) 3647–3667.
[11] A.F. Rakotondrainibe, J.A. Jeevarajan, A.J. Appleby, F.E. Little, The Electrochemical Society 193rd Meeting Abstracts, San Diego, 98-1 March 1998.
[12] M. Doyle, J. Newman, A.S. Gozdz, C.N. Schmutz, J.M. Tarascon, J. Electrochem. Soc. 143 (1996) 1890.
[13] S. Al Hallaj, J. Prakash, J.R. Selman, J. Electrochem. Soc., 1999, in press.